



The effect of liquid properties on the release of gas from bursting bubbles

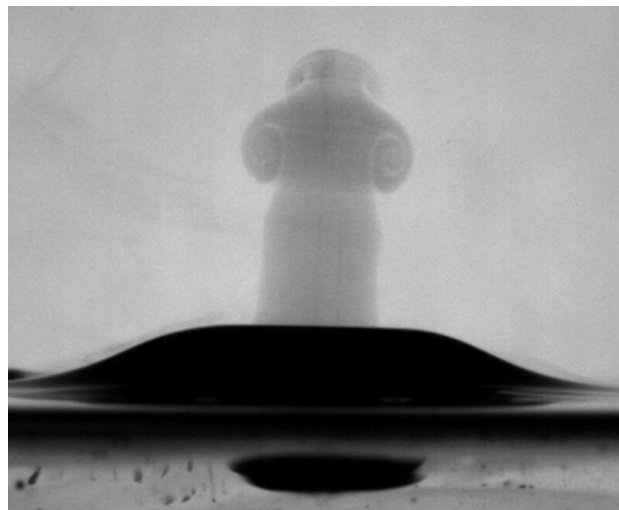
Ali A. Dasouqi¹ · Joe Ghossein² · David W. Murphy¹

Received: 4 December 2020 / Revised: 3 January 2022 / Accepted: 8 January 2022 / Published online: 29 January 2022
© The Author(s), under exclusive licence to Springer-Verlag GmbH Germany, part of Springer Nature 2022

Abstract

Bubbles are ubiquitous in industrial and environmental processes, and bubble bursting is a widely studied and highly important physical process. Bubbles bursting at an air–water interface may produce high-speed gas jets and vortex rings. Here, the effect of liquid properties such as viscosity, density, and surface tension on these gas jets is examined using high-speed visualization. Bursting events are examined for 500 μm to 44 mm diameter smoke-filled bubbles in five different liquids with variations in viscosity (1–944 mPa.s), surface tension (23.3–70.7 mN/m), and density (789–1259 kg/m³). Gas jet speed generally increases with parent bubble size until a bubble Bond number Bo of approximately one and subsequently increases at a slower rate. Further, gas jet speed correlates with surface tension, with low surface tension liquids such as ethanol producing low-speed jets and high surface tension liquids such as water producing high-speed jets. Film retraction speed decreases with increasing bubble size and, in conjunction with bubble emergence, influences gas jet diameter. A new scaling law relating the pressure potential energy of the parent bubble to the kinetic energy of the emerging gas jet reveals that bubble size and surface tension control the gas jet size and speed whereas liquid viscosity and density do not significantly affect jet behavior. This scaling is compared to a previously developed scaling for the gas jet Reynolds number. The prevalence of jet drop production, which heavily depends on liquid viscosity, also is examined as a function of Bo and bubble Ohnesorge number Oh_b .

Graphical abstract



✉ David W. Murphy
davidmurphy@usf.edu

¹ Department of Mechanical Engineering, University of South Florida, Tampa, FL 33620, USA

² Kevin T. Crofton Department of Aerospace and Ocean Engineering, Virginia Tech, Blacksburg, VA 24061, USA

1 Introduction

The bursting of bubbles at an air–liquid interface is an important physical process in many environmental and industrial applications. Bubble bursting has implications for climate (e.g., marine aerosol formation; Veron 2015), human respiratory health (e.g., aerosolization of harmful substances; Murphy et al. 2015; Prather et al. 2013), food science (e.g., beer and champagne bubbles; Liger-Belair et al. 2009), industry (e.g., processes such as gas fluxing and electrowinning; Zhang et al. 2011), and volcanology (e.g., Strombolian eruptions; Kobayashi et al. 2010; Chojnicki et al. 2015). Due to its tremendous importance and its diversity of applications, various aspects of the fluid dynamics of bubble bursting have long been studied. Much of the early work on this topic was motivated by a desire to understand the mechanisms of marine aerosol production and thus focused on the liquid component, namely the bubble cap film rupture and retraction and the generation of liquid droplets (e.g., jet drops and film drops) (Stuhlman 1932; Kientzler et al. 1954; Newitt et al. 1954; Mason 1957; Day and Lease 1968). Jet drops are ejected from the stem of the Worthington jet generated by the upward collapse of the cavity left by a bursting bubble whereas film drops are generated by the violent destruction of the thin film comprising the bubble cap. Extensive research has focused on jet drop generation (Duchemin et al. 2002; Ghabache et al. 2014; Walls et al. 2015; Ghabache and Séon 2016; Krishnan et al. 2017; Gañán-Calvo 2017, 2018; Deike et al. 2018; Lai et al. 2018; Brasz et al. 2018; Gordillo and Rodríguez-Rodríguez 2019; Blanco-Rodríguez and Gordillo 2020; Berny et al. 2020), hole initiation in bursting bubbles (Lhuissier and Villermaux 2012; Poulain et al. 2018), and the role of viscosity in the retraction of bubble cap films (Savva and Bush 2009).

In contrast, the fluid dynamics of the pressurized gas escaping from inside the bursting bubble is not well understood. Several early studies noted the formation of a vortex ring released from a bursting bubble (Rogers 1858; Swinton and Beale 1917), and Newitt et al. (1954) first photographed this phenomenon. Other researchers examined this flow as a possible mechanism for lofting tiny marine aerosol droplets into the atmosphere (Newitt et al. 1954; Blanchard 1963; Iacono and Blanchard 1987) or for lofting the aroma of carbonated beverages to the consumer (Singh and Das 2021). Recently, Dasouqi and Murphy (2020) and Dasouqi et al. (2020) used high-speed stereophotogrammetry to study this gas escape behavior for bubbles of various sizes (e.g., 440 μm –4 cm) bursting at an air–water surface and presented measurements of the gas jet and vortex ring characteristics. Indeed, their measurements showed that the initial speed of the gas jet sharply

increases with parent bubble size until the bubble Bond number reaches unity and subsequently increases at a slower rate. In that investigation, these researchers also presented flow visualization results which explain how film retraction speed, which is correlated with bubble size, affects the initial speed of the gas jet. Specifically, the high film retraction speeds characteristic of smaller bubbles produced correspondingly slower jets emitted through relatively larger openings whereas the low film retraction speeds characteristic of larger bubbles produced correspondingly higher jet speeds emitted through relatively smaller openings. In addition, a simple scaling relationship of $Re_{jet} = 126Bo^{0.5}$ was proposed to relate the Reynolds number of the emerging gas jet to the parent bubble Bond number. Here, gas jet Reynolds number is defined as $Re_{jet} = \frac{V_{jet}D_{jet}}{\nu_g}$, and Bond number is defined as $Bo = \frac{\rho_l g R^2}{\sigma}$, where V_{jet} is the speed of the emerging gas jet, D_{jet} is the gas jet frontal diameter, $\nu_g = 1.5 \times 10^{-5} \text{ m}^2/\text{s}$ is the kinematic viscosity of the gas (air at 21 °C), ρ_l is liquid density, $g = 9.81 \text{ m/s}^2$ is the gravitational constant, R is the bubble equivalent radius, and σ is the fluid surface tension. They concluded that large bubbles eject high-speed, high Reynolds number jets which slowly decay and which roll up into fast-growing, highly oblate vortex rings which travel far. In contrast, small bubbles eject low-speed, low Reynolds number jets which quickly decay and which roll up into slow-growing, spherical vortex rings which travel short distances. In the same vein, Singh and Das (2019) performed simulations which examined the airflow exiting the cavity formed by a collapsing bubble but did not examine the gas jet initially ejected upon bursting. Singh and Das (2021) subsequently examined air flow exiting bursting bubbles at $Bo = 0.058$ –4, reproduced many of the gas jet flow features found by Dasouqi et al. (2020), and also investigated the effects of nearby human inhalation and asymmetric bubble perforation.

While Dasouqi et al. (2020) showed the effect of bubble size on gas jet and vortex ring properties, the effect of fluid properties such as liquid density, liquid viscosity μ_l , and surface tension on gas escape from bursting bubbles is not well understood. Variations in liquid density and surface tension will affect both the initial bubble shape through Bo and the film retraction speed, and Dasouqi et al. (2020) found that film retraction speed affected gas jet speed for air bubbles bursting in water. Other researchers have examined the gas released from inside large soap bubbles with low surface tension and observed correspondingly slower gas jet speeds (Buchholz and Sigurdson 2000, 2002; Jaw et al. 2007; Torikai et al. 2011; Murashita et al. 2012; Kim et al. 2014). Variations in liquid viscosity also may impact film retraction. Researchers investigating highly viscous film retraction found the absence of a rim on the film edge and a delay

in the transient acceleration caused by viscous forces, after which the film attained a constant retraction speed (Debrégeas et al. 1995; Savva and Bush 2009). The potential effects of these viscosity-related phenomena on gas escape from bursting bubbles also are not known.

Here, we use high-speed visualization to examine the effects of bubble size and liquid properties (e.g., density, viscosity, and surface tension) on the formation of gas jets and vortex rings emerging from bubbles bursting at an air–liquid interface. We vary the bubble size and fluid properties to consider the effects of viscosity (1–944 mPa.s), surface tension (23.3 – 70.7 mN/m), and density (789–1259 kg/m³). We present measurements of the gas jet and characteristics of the retraction of the parent bubble cap film and relate these quantities to the gas jet Reynolds number, bubble Bond number, film Ohnesorge number $Oh_f = \frac{\mu_l}{\sqrt{2h\rho\sigma}}$, and bubble Ohnesorge number $Oh_b = \frac{\mu_l}{\sqrt{\rho_l\sigma R}}$, where h is the film thickness.

2 Experimental methods

An experimental setup similar to that of Dasouqi et al. (2020) used for studying water bubbles was used to study the emerging gas jets produced by bursting bubbles in four additional liquids with varying surface tensions, viscosities, and densities. Whereas that setup comprised a stereophotogrammetry system with two synchronized and orthogonally positioned high-speed cameras used to measure gas jet parameters in three dimensions, an alternative setup comprising a single high-speed camera was used here to measure two-dimensional (projected) parameters. Briefly, a rectangular acrylic tank (10.2 × 10.2 × 15.2 cm³) was filled to the brim with one of four liquids, namely ethanol, soapy water (at a concentration of 0.4 mg soap/ml water using Alconox powder soap), engine oil (5 W-30, Pennzoil), or glycerol (Nature's Oil). Single bubbles ranging in diameter from approximately 500 μm–44 mm were produced at a constant rate by a programmable syringe pump (New Era Pump Systems Inc.) injecting smoky air through nozzle tips of various diameters inserted through a bulkhead fitting in the bottom of the acrylic tank. The tank was lifted by an elevating table (Velmex B29) in order to facilitate visualization.

The bubbles were allowed to age and burst naturally. Smoke for visualization was produced by a custom-built cold smoke generator or fog machine (Theefun) and was captured in a 60 ml syringe prior to injection.

The surface tension of each liquid was measured using the pendant drop method (the average of 5 measurements; Song and Springer 1996). Liquid viscosity was measured using various Cannon Fenske viscometers. The physical properties of the five fluids are listed in Table 1, with values for water taken from Dasouqi et al. (2020). It is worth noting that the surface tension of the soapy water solution (38.9 ± 0.84 mN/m) is somewhat higher than values found in the literature. This higher value can be attributed to the low soap concentration which was chosen to limit the formation of coalesced foamy bubbles on the water surface. Soapy water was chosen as a working fluid to investigate the potential effect of surfactants on the gas release process. Density values for engine oil, glycerol, and ethanol were taken from manufacturer specifications. Soapy water density was measured with a densitometer (Anton-Paar-Str.20). Table 1 also shows the capillary length a of each fluid, where $a = \sqrt{\frac{\sigma}{\rho_l g}}$.

The bursting bubbles were visualized by a single high-speed camera (Photron FASTCAM SA-Z) recording at 10–20 kHz with a spatial resolution of 1024 × 1024 pixels. Backlighting was provided by an LED light (Nila NINZLB). Several fields of view (from 15 × 15 mm to 78 × 78 mm) were employed according to the bubble size, with the spatial resolutions varying accordingly from 15–76 μm/pixel. The camera was calibrated both above and below the liquid surface using a transparent microslide ruler with the focal plane positioned at the center of the tank. The camera was set to a post-trigger configuration, and, upon observing a bubble bursting within the focal plane, was manually triggered.

Approximately a hundred bursting events were observed for each liquid, and about forty videos for each liquid in which the bubble was well focused were selected for further analysis. The recorded videos then were processed in ImageJ software (NIH) following the method of Dasouqi et al. (2020). Briefly, the bubble size was first characterized following a similar approach to that of Teixeira et al. (2015). The bubble equivalent diameter $2R$, the diameter of a sphere with the same enclosed volume as the hemispherical bubble, is used to represent bubble size for large

Table 1 Values of physical properties of liquids used in the experiments at 20 °C. Values for water are taken from Dasouqi et al. (2020)

Fluid		Water	Soapy Water	Ethanol	Engine Oil 5W30	Glycerin
Property	Unit					
Surface Tension (σ)	mN/m	70.7	38.9	23.3	32.2	63.9
Dynamic Viscosity (μ_l)	mPa.s	1	1	1.1	55	944
Density (ρ)	kg/m ³	998	998	789	859	1259
Capillary Length (a)	mm	2.69	1.99	1.74	1.95	2.28

bubbles. For small bubbles residing mostly beneath the surface, the bubble diameter was directly measured and is reported as $2R$. For each recorded event, the frame at which bursting initiated was set as time $t = 0$. For each bursting bubble, a single point on the tip of the retracting film was manually tracked over $t = 0.3\text{--}0.5$ ms from which a measured distance could be divided by the elapsed time to calculate film retraction speed V_{fr} . However, for the smallest bubbles, the last-measured film retraction speed was used due to complete destruction of the film prior to $t = 0.5$ ms. The film thickness h was theoretically calculated using the Taylor–Culick equation $V_{fr} = \sqrt{2\sigma/\rho_l h}$ (Taylor 1959; Culick 1960; Brenner and Gueyffier 1999; Savva and Bush 2009; Pierson et al. 2020). Further, the forward displacement of the gas jet front after emerging from the enlarging hole in the bubble film was similarly tracked over $t = 0.3\text{--}0.5$ ms in order to calculate gas jet speed V_{jet} at $t = 0.4$ ms. Finally, the gas jet frontal diameter D_{jet} was measured at $t = 0.4$ ms, thus allowing calculation of Re_{jet} . The time point of $t = 0.4$ ms was chosen because it was the earliest possible time point at which the gas jet properties could reliably be measured for all bubble sizes of all working fluids. It is important to note that measurements for water were acquired using a 3D stereophotogrammetry system (Dasouqi et al. 2020) whereas those presented here for ethanol, soapy water, engine oil, and glycerol were acquired using a single camera. The bubbles formed by engine oil and glycerol largely burst vertically in the plane of focus and thus did not require 3D measurements. The ethanol and soapy water bubbles did not necessarily burst vertically, and thus more scatter is seen in these data. Finally, as it was difficult to obtain single ethanol bubbles with $2R > \sim 14$ mm, several videos in which a smaller adjacent bubble was present were included in the analysis for this size range.

3 Results and discussion

3.1 Flow visualization

Flow visualization of the bursting of large ($Bo > \sim 10$), medium ($1.3 < Bo < 3.7$), and small ($0.1 < Bo < 0.2$) bubbles is now presented, with the corresponding values of $2R$, Bo , Oh_b , and Oh_f shown in Table 2. Figure 1(a–e) shows a sequence of images illustrating the bursting of large smoke-filled bubbles resting on water, soapy water, ethanol, engine oil, and glycerin fluid surfaces, respectively. Prior to bursting ($t = -2$ ms), bubble shape is governed by Bo , which describes bubble size, fluid density, gravity, surface tension, and the pressure difference across its film interface ΔP , and can be determined analytically by solving the static Young–Laplace equation (Toba 1959, Lhuissier and Villermaux 2012, Teixeira et al. 2015, Deike et al. 2018, Berny et al. 2020). For example, the engine oil bubble in Fig. 1(d) has low curvature due to its extremely high Bo whereas the other bubbles in Fig. 1 have higher film curvatures which reflect their correspondingly lower Bond numbers. At $t = 0.5$ ms, a hole opens in each bubble cap film, and a smoke jet emerges at speeds of 4.13 m/s, 2.75 m/s, 1.1 m/s, 4.12 m/s, and 3.60 m/s for water, soapy water, ethanol, engine oil, and glycerin, respectively. The hole diameter for water, soapy water, engine oil, and glycerin is 2–3 mm, but the ethanol hole diameter is ~ 5 mm owing to its fast film retraction. Specifically, the film edge retracts at speeds of 2.51 m/s, 0.57 m/s, 3.76 m/s, 0.81 m/s, and 1.68 m/s, respectively. The gas jet front, which has begun rolling up into a vortex ring for water, engine oil, and glycerin at $t = 2$ ms, decreases to speeds of 3.52 m/s, 2.07 m/s, 1.05 m/s, 2.39 m/s, and 2.91 m/s, respectively. At $t = 5$ ms, the bubble film has almost completely collapsed into the surrounding fluid in the water, soapy water, and ethanol cases but is still slowly retracting for the engine oil

Table 2 Values of parent bubble Bond number Bo , film Ohnesorge number Oh_f , and bubble Ohnesorge number Oh_b for the differently sized bubbles bursting in five different working fluids, corresponding to Figs. 1, 2 and 3

Size	Parameter	Water	Fluid			
			Soapy Water	Ethanol	Engine Oil	Glycerin
Large	$2R$ (mm)	26.6	23.5	12.9	29.9	26.0
	Bo	24.5	34.6	13.8	58.5	32.6
	Oh_f	0.001	0.007	0.09	0.691	12.33
	Oh_b	0.001	0.001	0.003	0.086	.923
Medium	$2R$ (mm)	6.4	6.8	6.7	7.1	6.9
	Bo	1.34	2.93	3.7	3.32	2.31
	Oh_f	0.031	0.033	0.09	1.815	24.08
	Oh_b	0.002	0.003	0.004	0.176	1.79
Small	$2R$ (mm)	1.78	1.55	1.58	1.28	1.51
	Bo	0.12	0.15	0.2	0.10	0.11
	Oh_f	0.042	0.039	0.14	3.282	40.33
	Oh_b	0.004	0.006	0.009	0.413	3.83

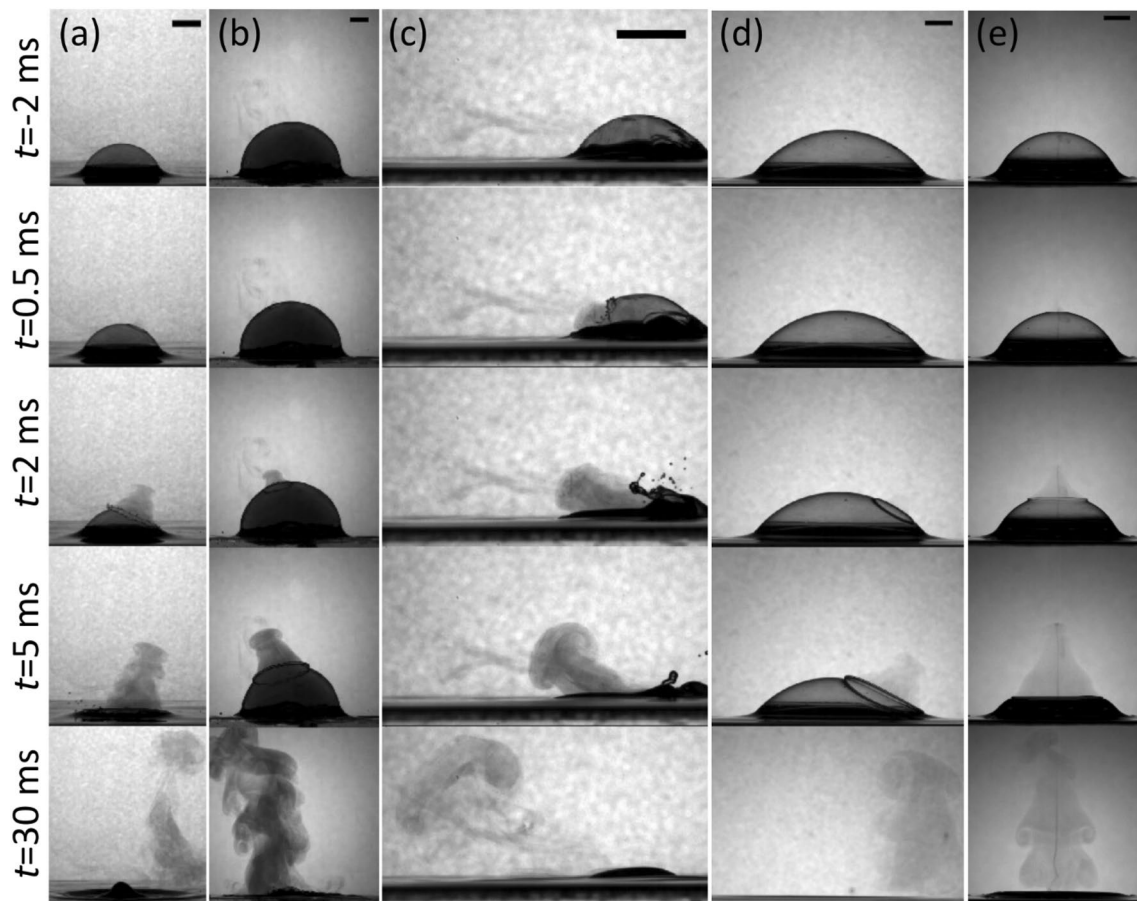


Fig. 1 Sample images from a time series showing the bursting of $2R=26.6$ mm, 23.5 mm, 12.9 mm, 29.9 mm, and 26.0 mm smoke-filled bubbles floating on (a) water, (b) soapy water, (c) ethanol, (d)

engine oil, and (e) glycerin surfaces, respectively, and the subsequent release of a gas jet. The hole in the bubble cap forms at $t=0$ ms. The scale bar in all images is 5 mm

bubble. The glycerin bubble collapses downward as it slowly retracts owing to its low surface tension and high density.

The gas jet has rolled up into a vortex ring at $t=5$ ms for all liquids except the soapy water, which has a low pressure difference driving the gas out of the bubble (Kim et al. 2014). The growing primary (i.e., first) vortex ring travels at speeds of 2.56 m/s for water, 0.78 m/s for ethanol, 1.57 m/s for engine oil, and 2.18 m/s for glycerin. Primary vortex ring size, characterized by the axial distance between vortex centers (Dasouqi et al. 2020), also differs between fluids owing to variations in the time of vortex formation and thus film retraction speed. For example, glycerin produces a small vortex ring because its slowly retracting film creates a small opening through which the gas escapes, leading to a relatively small jet and vortex ring. Further, in each case, the smoke jet diameter increases moving downwards from the primary vortex ring, if present, towards the bursting bubble, which reflects the smoke being emitted through a growing aperture. The water bubble produces multiple Kelvin–Helmholtz

vortices along the edge of its smoke jet as the liquid film rapidly retracts over the surface of the smoke within the bubble, an effect also seen in ethanol. At this time point, these multiple vortices are absent for the other fluids, for which the film retracts more slowly.

At $t=30$ ms, the smoke jet produced by the soapy water bubble has finally rolled up into a disorganized vortex ring. The primary vortex rings have grown substantially and travel at speeds of 1.27 m/s, 0.38 m/s, 0.42 m/s, 0.61 m/s, and 1.05 m/s for the water, soapy water, ethanol, engine oil, and glycerin cases, respectively. The vortex rings produced from the ethanol and engine oil bubbles are somewhat lopsided owing to the fact that the bubble bursting originated towards the bubble's side. The high-speed vortex ring produced from water has almost completely pinched off from its disorganized trailing flow. In contrast, well-organized vortices are present along the edges of the smoke jets produced by the more viscous liquids owing to their slower film retraction speeds.

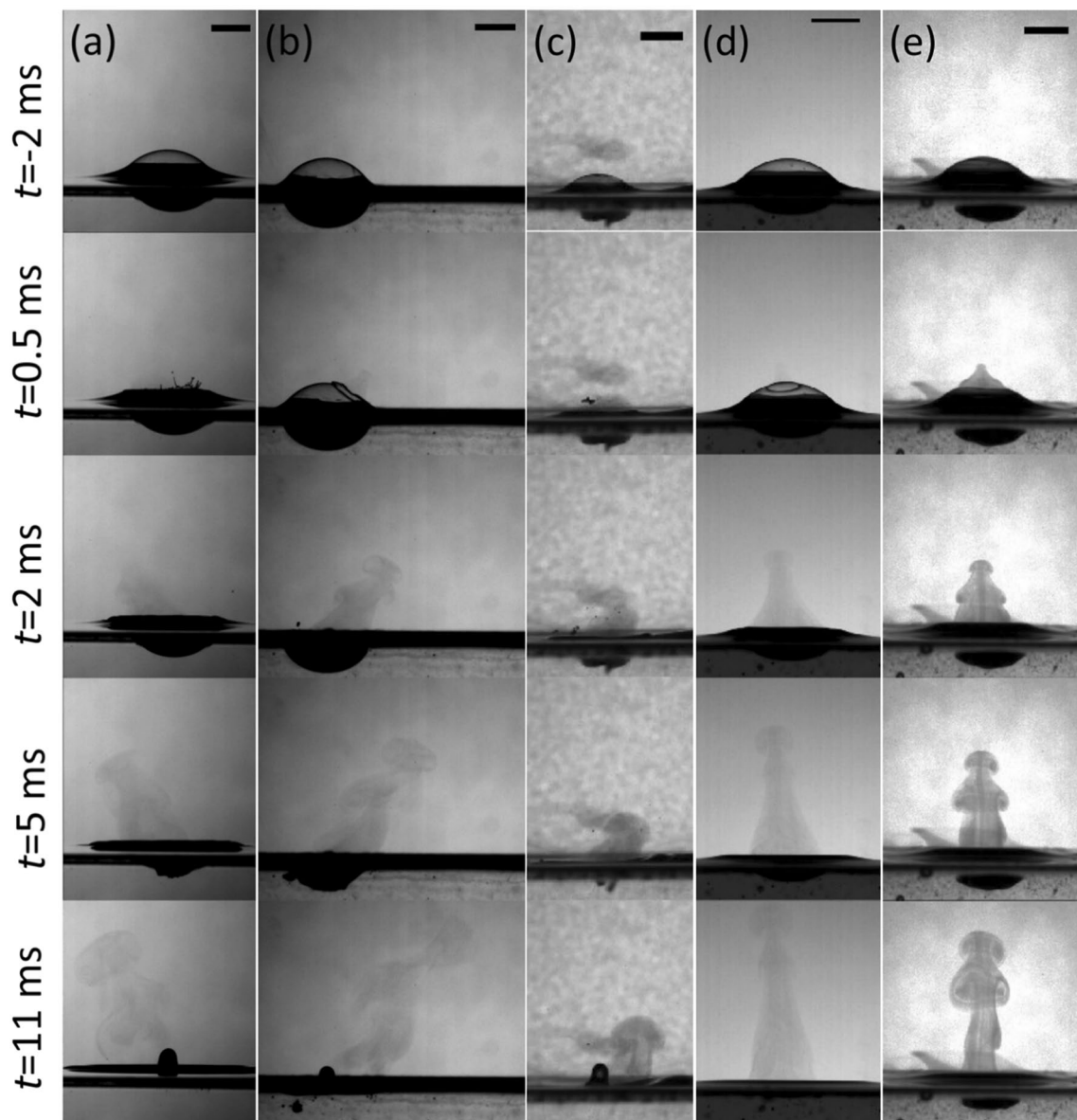


Fig. 2 Sample images from a time series showing the bursting of $2R=6.4$ mm, 6.8 mm, 7.1 mm, and 6.9 mm smoke-filled bubbles floating on (a) water, (b) soapy water, (c) ethanol, (d) engine

oil, and (e) glycerin surfaces, respectively, and the subsequent release of a gas jet. The hole in the bubble cap forms at $t=0$ ms. The scale bar in all images is 3 mm

Figure 2(a–e) shows a sequence of images illustrating the bursting of medium-sized smoke-filled bubbles resting atop water, soapy water, ethanol, engine oil, and glycerin surfaces. At $t=0.5$ ms, the water and ethanol bubble films have almost completely collapsed into the surrounding water, and both have generated film drops due to the high film retraction speed. A smoke jet emerges through the expanding hole at speeds of 3.12 m/s, 1.01 m/s, 1.65 m/s, 2.14 m/s, and 1.67 m/s, for water, soapy water, ethanol, engine oil, and glycerin, respectively. Film retraction speeds are 4.37 m/s, 1.83 m/s, 2.13 m/s, and 3.27 m/s for water, soapy water, engine oil, and glycerin, respectively.

The ethanol film is already almost completely retracted at this time and has $V_{fr}=3.82$ m/s at a slightly earlier time point ($t=0.2$ ms). The film retraction speeds correspond to hole diameters of 2.49 mm, 2.02 mm, and 3.07 mm diameter in soapy water, engine oil, and glycerin, respectively. Smoke jet shape is affected by the film retraction behavior. For example, the conical smoke jets emitted from soapy water and engine oil bubbles are due to the slower opening of their holes whereas the nipple-like shape of the glycerin bubble smoke jet may be due to the downward collapse of the bubble cap owing to its high density.

By $t=2$ ms, primary vortices have been formed for all fluids except the low velocity gas jet emitted from the ethanol bubble, and all bubble films have been destroyed. The speed of the gas jet front decreases to 2.16 m/s, 0.75 m/s, 1.51 m/s, 1.89 m/s, and 1.37 m/s for water, soapy water, ethanol, engine oil, and glycerin, respectively. A secondary wider vortex is seen for all liquids except ethanol, for which a secondary vortex ring does not form, and engine oil, for which this secondary vortex ring forms later. The source of the secondary vortex may be related to the fast upward collapse of the cavity (e.g., for water) and to the interaction of the retracting film and the gas jet for the other cases (Dasouqi et al. 2020). At $t=5$ ms, the bubble cavity continues to collapse upward which further expels a smoke jet at low speeds. At $t=11$ ms, the primary vortex ring formed in the water, soapy water, and ethanol cases has grown substantially whereas growth in the other two cases is much slower. Finally, a Worthington jet protruding above the bath surface is seen in the water, soapy water, and ethanol cases, though no jet drop is formed (Gekle and Gordillo 2010). In contrast, the high viscosity of engine oil and glycerin causes a slow collapse of the bubble cavity which inhibits Worthington jet formation. The absence of the Worthington jet allows the stem of the gas jet to remain undisturbed and “attached” to the bath surface.

Figure 3(a–e) shows a sequence of images illustrating the bursting of small smoke-filled bubbles resting atop water, soapy water, ethanol, engine oil, and glycerin surfaces. These low Bo bubbles are more spherical and maintain a higher pressure difference with the atmosphere ($\Delta P > 100$ Pa). After bursting ($t=0$ ms), the film retracts at a speed of 5.94 m/s for water, 3.03 m/s for soapy water, 5.86 m/s for ethanol, 3.84 m/s for engine oil, and 5.46 m/s for glycerin. At $t=0.5$ ms, the bubble film has fully retracted in all bubbles and a gas jet has emerged with respective speeds of 1.31 m/s, 0.66 m/s, 0.61 m/s, 1.06 m/s, and 1.07 m/s. Film drops are ejected nearly horizontal to the surface for the water bubble due to the low Oh_f . At $t=2$ ms, the speed of the smoke jet decreases to 0.71 m/s for water, 0.33 m/s for soapy water, 0.47 m/s for ethanol, 0.59 m/s for engine oil, and 0.57 m/s for glycerin. Further, for all fluids except ethanol, the leading edge has begun to roll up into a vortex ring which is smaller than the width of the jet where it emerges from the bubble. For ethanol, the low velocity gas jet does not begin to roll up into a vortex ring until later. In addition, a Worthington jet has already been generated for the soapy water and ethanol at this point, whereas the cavities of the more viscous fluids collapse upwards more slowly.

At $t=5$ ms, the smoke jet has rolled up into a vortex ring which travels upward at a speed of 0.46 m/s, 0.11 m/s, 0.28 m/s, and 0.19 m/s for water, soapy water, engine oil, and glycerin, respectively. The gas jet produced from ethanol has yet to form a vortex ring. The primary vortex produced

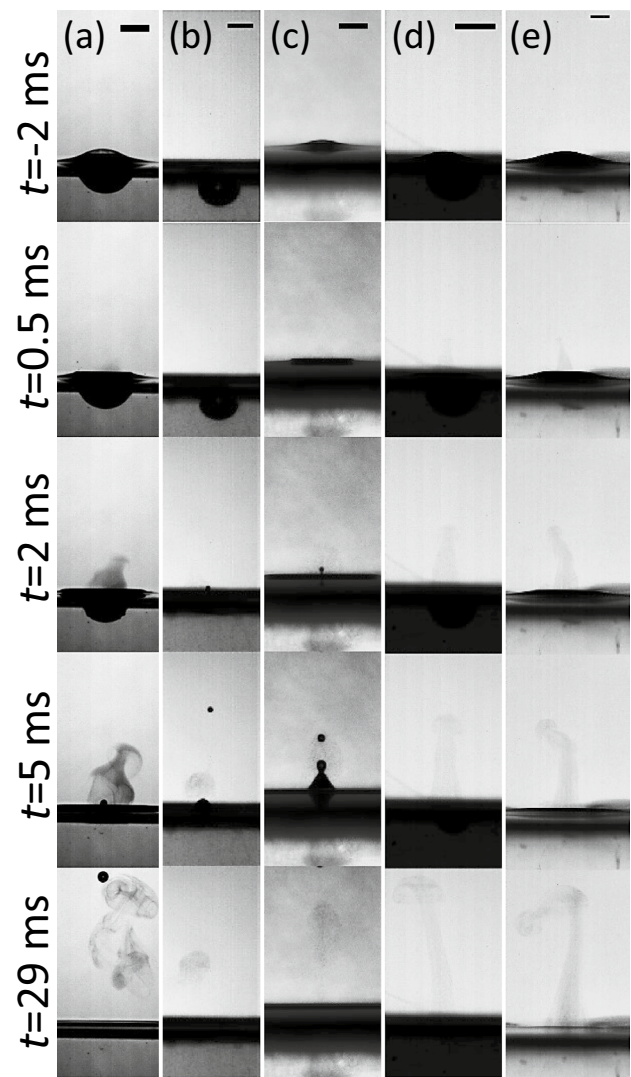


Fig. 3 Sample images from a time series showing the bursting of $2R=1.78$ mm, 1.55 mm, 1.58 mm, 1.28 mm, and 1.51 mm smoke-filled bubbles floating on (a) water, (b) soapy water, (c) ethanol, (d) engine oil, and (e) glycerin surfaces, respectively, and the subsequent release of a gas jet. The hole in the bubble cap forms at $t=0$ ms. The scale bar in all images is 1 mm

by the glycerin bubble has hooked to the left as the fast-moving smoke being expelled from the upwards collapsing cavity seems to overtake the primary vortex ring and subsequently forms a secondary vortex ring comparable in size to the primary vortex ring. In each case, the base of the smoke column continues to expand as smoke is expelled from the initial cavity by the rise of the liquid surface. Indeed, the subsurface cavity is no longer visible for water as a Worthington jet reaches above the water surface. In the soapy water case, the Worthington jet has ejected a single jet drop at a speed of 1.16 m/s, and the ethanol bubble has ejected two jet drops which travel upwards through the gas jet. The subsurface cavity is still collapsing upward for engine oil

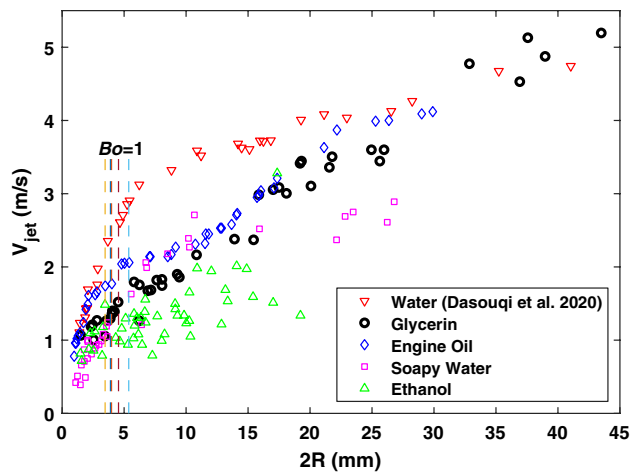


Fig. 4 Gas jet front speed V_{jet} as a function of bubble equivalent diameter $2R$ measured at $t=0.4$ ms after hole nucleation ($t=0$ ms) for five different liquids

and glycerin at this time point. At $t=29$ ms, the speed of the primary vortex ring has become negligible for all cases, and, in the water case, a jet drop has pinched off the Worthington jet, which has fallen back onto the water surface.

Finally, it is interesting to note that the retracting film edges acquire various shapes according to Oh_f . For example, the water, soapy water, and ethanol bubble films display a thickened rim and a crown of ligaments owing to a Rayleigh–Taylor instability, and both fall into the low Oh_f regime in which film retraction is inertia-dominated and capillary wave disturbances are generated ahead of the retracting rim (Savva and Bush 2009). The engine oil bubbles fall into the medium Oh_f regime where the instabilities on the receding rim disappear owing to the higher viscosity of the fluid (Savva and Bush 2009). The glycerin bubbles correspond to the high Oh_f regime where no fluid seems to collect in the receding edge because of the dominating force of viscosity (Savva and Bush 2009). These differences in film edge morphology, which are unlikely to affect the gas jet, were observed for the large and medium bubbles but could not be visualized in the small bubbles owing to insufficient spatial resolution.

3.2 Gas jet characterization

Figure 4 shows the relation between $2R$ and V_{jet} at $t=0.4$ ms after hole nucleation for all working fluids, where data for water are taken from Dasouqi et al. (2020). Gas jet velocity increased with bubble size for all fluids, but the trends for each fluid will be discussed separately. As described by Dasouqi et al. (2020), the gas jet speed for water bubbles increases with bubble size until $2R=5.44$ mm and then increases at a lower rate. This break in slope occurs at $Bo \sim 1$, where gravity balances surface tension (i.e., when

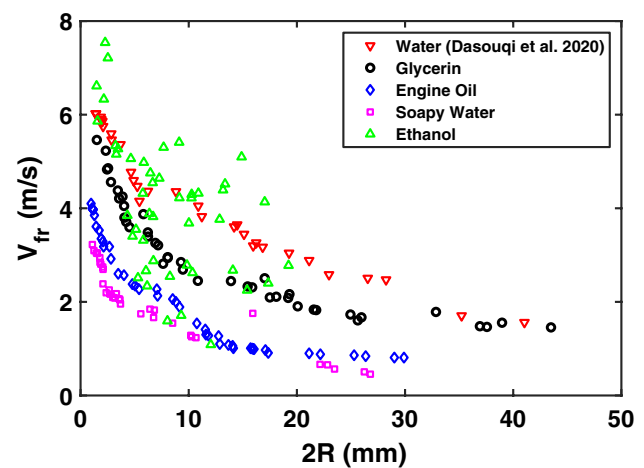


Fig. 5 Film retraction speed V_{fr} as a function of bubble equivalent diameter $2R$ measured at $t=0.4$ ms after hole nucleation ($t=0$ ms) for five different liquids

the bubble radius of curvature equals the capillary length). Physically, this break corresponds to greater emergence of larger bubbles from the water surface. Further, Fig. 5 shows that V_{fr} decreases as $2R$ increases. Dasouqi et al. (2020) also showed how gas jet speed is linked to the film thickness and retraction speed. Tiny, high pressure bubbles expel air at low speeds through fast-opening apertures in thin films that are large relative to the bubble size. Indeed, for small bubbles which are largely submerged, the aperture through which gas is released may equal the original area of the bubble film cap. Conversely, large, low pressure bubbles expel air at high speeds through slow-opening apertures in thick films that are small relative to the bubble size. Since V_{fr} decreases as $2R$ increases, it might be expected that the gas jet diameter would also decrease as $2R$ increases. However, Fig. 6 shows that gas jet diameter counterintuitively increases with $2R$. For water bubbles, gas jet diameter increases from a minimum of $D_{jet} \sim 340$ μm at $2R=1.39$ mm and subsequently plateaus at $D_{jet} \sim 1.8$ mm for $2R=20$ mm. One possible reason for this trend is that gas jet diameters for very small bubbles may be limited by their submergence and the resulting small initial area of their bubble cap film through which the gas jet may emerge (e.g., Fig. 6 in Dasouqi et al. (2020)). The emergence of larger bubbles above the water surface would then allow the formation of sufficient film cap area for larger holes to develop and larger gas jets to be emitted. For sufficiently large bubbles, the hole in the bubble film would be able to expand unimpeded by the surrounding water surface, leading to larger diameter gas jets. However, the tendency to larger gas jet diameters is counterbalanced by the decrease in film retraction speed for larger bubbles, which explains why gas jet diameter eventually plateaus.

For soapy water, Fig. 4 shows that a similar break in slope occurs close to $Bo=1$ (corresponding to $2R=3.98$ mm),

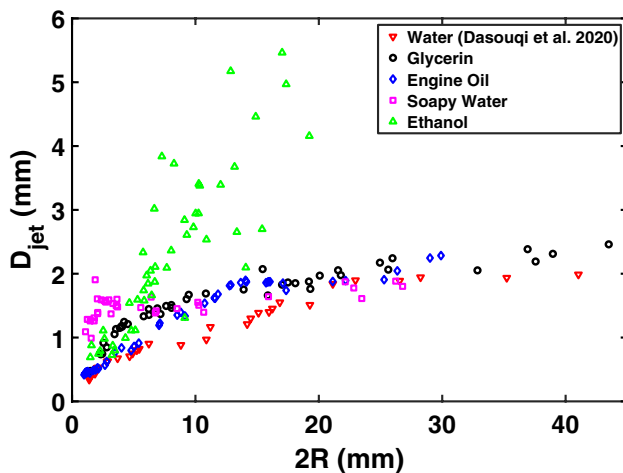


Fig. 6 Measured values of the gas jet frontal diameter D_{jet} at $t=0.4$ ms as a function of bubble equivalent diameter $2R$ for five different liquids

though scatter in the data makes it difficult to pinpoint. Jet speeds for soapy water bubbles were lower than those of the water bubbles. For example, in Fig. 2 the water bubble ($2R=6.4$ mm) produced a jet speed of 3.12 m/s whereas a soapy water bubble of approximately the same size ($2R=6.8$ mm) produced a lower jet speed of 1.01 m/s. These lower jet speeds reflect the lower pressures sustained inside of the soapy water bubbles owing to the lower liquid surface tension. Further, Fig. 5 shows that V_{fr} is lower for soapy water than for water, though both follow the same trend. Compared to water, the lower film retraction speeds of soapy water translate into smaller apertures through which the jet may be ejected but do not translate into higher jet speeds owing to the lower driving force (i.e., lower surface tension). However, Fig. 6 shows that the gas jet diameters for the small soapy water bubbles are greater than those of similarly sized water bubbles. This difference is likely because the soapy water bubbles are less submerged, again owing to their lower surface tension, which generates a larger bubble cap film area available to form larger apertures through which larger diameter jets may be ejected. For bubbles larger than approximately $2R=20$ mm, however, gas jets emitted from soapy water bubbles are slightly smaller than those emitted from water bubbles likely owing to the lower film retraction speeds of soapy water.

Figure 4 shows that the ethanol bubbles have the lowest gas jet speeds, which reflect ethanol's extremely low surface tension and the large diameter openings generated by fast film retraction. Further, there is substantially more scatter in these data as the bursting events occur on a shorter time scale and are more violent. Owing to the difficulty in producing tiny, smoke-filled ethanol bubbles, not enough data could be acquired in the $Bo < 1$ range to determine if a change in

slope occurred at $Bo=1$ (corresponding to $2R=3.47$ mm). Further, Fig. 5 shows that the ethanol films generally had the highest film retraction speeds, with a maximum $V_{fr}=9.1$ m/s for a $2R=2.62$ mm bubble. These extremely high speeds reflect the thin nature of these films, many with sub-micron film thicknesses. As shown in Fig. 6, these high values of V_{fr} translated into large openings in the film and thus into large values of D_{jet} , with some jet diameters reaching as large as 5.5 mm at this time point.

Results from engine oil and glycerin bubbles are fairly similar and will be discussed together. Figure 4 shows that the trend in gas jet speed with increasing bubble size for both these fluids is similar to that of the water and soapy water bubbles. The engine oil bubbles had a break in slope occurring at approximately $2R=3$ mm, which again closely corresponds to the bubble size where $Bo=1$ ($2R=3.90$ mm). However, no distinct break in the slope was seen in jet speeds produced from glycerin bubbles, though this break would be expected to occur at $2R=4.74$ mm (corresponding to $Bo=1$). This may be because of the sparsity of data acquired for the smallest bubbles due to the difficulty in producing tiny smoke-filled bubbles. Gas jet speeds emitted from engine oil and glycerin bubbles are generally lower than those emitted from water bubbles but greater than those emitted from soapy water bubbles. Further, Fig. 5 shows that the engine oil and glycerin film retraction speeds also lie between those of water and soapy water, though the speeds for engine oil are less than those of glycerin owing to the lower surface tension of glycerin. Figure 6 shows that the jet diameters are also generally intermediate between those of water and soapy water. These results illustrate that increasing the viscosity by one or even two orders of magnitude does not significantly affect the processes generating the gas jet from the bursting bubble, a point that will subsequently be discussed in more detail.

3.3 Scaling

Dasouqi et al. (2020) found a scaling relationship of $Re_{jet}=126Bo^{0.5}$ (equivalent to $Re_{jet}=126R/a$) between the parent bubble Bond number and the Reynolds number of the resulting gas jet released from the bursting bubble using water as the working fluid. Figure 7 shows that this relationship also holds reasonably well for all investigated fluids with a few exceptions. For example, Re_{jet} is somewhat lower than predicted for the highest Bond number bubbles (e.g., $Bo > \sim 10$) for all fluids, a trend also noted by Dasouqi et al. (2020). This departure is particularly evident for soapy water, which may possibly be related to surfactants, though, overall, surfactants do not seem to have a major effect on the gas jet. In addition, Re_{jet} for engine oil is systematically lower than predicted by the scaling line but seems to also hold to a $Bo^{0.5}$ relationship, though with a smaller prefactor.

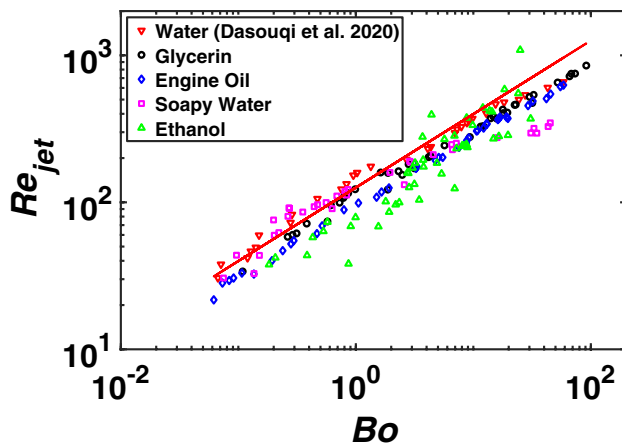


Fig. 7 Reynolds number of the emerging gas jet at $t=0.4$ ms as a function of the parent bubble Bond number for five different liquids. The line shows the scaling relationship $Re_{jet} = 126Bo^{0.5}$ previously found by Dasouqi et al. (2020) for water

The data for ethanol, though limited to a narrower Bo range than the other fluids and having a greater amount of scatter, also follow the original scaling reasonably well.

This scaling relationship describes the initial momentum of the emerging gas jet in terms of the fluid surface tension, density, gravity, and bubble size. Notably, liquid viscosity, which varied by almost a thousandfold, does not significantly affect the scaling. This makes sense because viscosity plays no role in the physical processes which may affect the gas jet formation. For example, film retraction speed is governed by the Taylor–Culick formula, which includes only the effects of fluid density, surface tension, and film thickness. Cavity collapse, Worthington jet, and jet drop formation are significantly affected by liquid viscosity through an Ohnesorge or Laplace number (Walls et al. 2015; Deike et al. 2018), but the initial gas jet release precedes these phenomena and is thus unaffected by liquid viscosity. Finally, liquid viscosity affects the morphology of the retracting film edge, but this also does not affect the initial gas jet momentum.

While providing insight into the lack of importance of liquid viscosity in gas jet behavior, a weakness of the scaling proposed by Dasouqi et al. (2020) is that it lacks a physical explanation. Further, the relative importance of all terms in the scaling is not clear since some physical parameters could not be experimentally varied (e.g., ν_g). Here, we propose an alternative scaling based on the idea that the kinetic energy of the gas jet emitted from the bursting bubble, $KE_{jet} \sim \frac{1}{2}m_{jet}V_{jet}^2$, should scale with the bubble’s potential energy from pressure, $PE_{pressure} \sim \Delta PV_B$. The potential energy (i.e., the product of bubble volume V_B and ΔP , the pressure difference between the bubble interior and atmosphere, which is given by the Young–Laplace equation) scales as $\sim \sigma R^2$. The mass of the air jet, which is assumed to

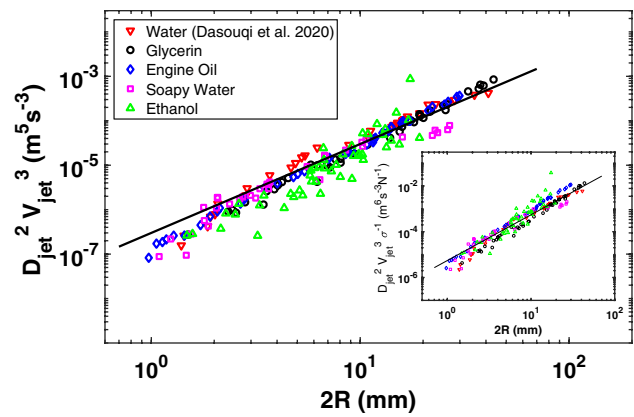


Fig. 8 Plot of the parameter $D_{jet}^2 V_{jet}^3$ as a function of parent bubble size $2R$ for five different liquids. Inset: Plot of the parameter $\frac{D_{jet}^2 V_{jet}^3}{\sigma^2}$ as a function of parent bubble size $2R$ for the same five liquids. In both plots, the solid line represents the R^2 scaling law

comprise a cylinder of air of diameter D_{jet} and length $L_{jet} = V_{jet}t$ at $t=0.4$ ms, scales as $m_{jet} \sim \rho_g D_{jet}^2 V_{jet}t$, where ρ_g is the density of air. The kinetic energy of the gas jet thus scales as $\sim \beta D_{jet}^2 V_{jet}^3$, where the prefactor β is the dimensional constant $\beta = \pi \rho_g t / 8$. A scaling law of $\beta D_{jet}^2 V_{jet}^3 \sim \sigma R^2$ is thus found. Figure 8 shows a plot of $2R$ vs $D_{jet}^2 V_{jet}^3$, where the solid line represents the R^2 scaling law. This plot shows that, even without considering surface tension, the data for all fluids follow the scaling law reasonably well. Including surface tension in the scaling by plotting $2R$ vs $\frac{D_{jet}^2 V_{jet}^3}{\sigma^2}$, as in the inset of Fig. 8, yields a slightly improved collapse onto a master curve. In accordance with $PE_{pressure} \sim \sigma R^2$, bubble size is thus shown to influence gas jet velocity more strongly than surface tension (e.g., Fig. 4). Surface tension may also play a secondary role in governing D_{jet} by controlling film retraction speed. This new scaling reveals that liquid density, which varied only slightly, and gas viscosity, which did not vary, did not significantly affect gas jet behavior and thus performs better than the $Bo-Re_{jet}$ scaling proposed by Dasouqi et al. (2020). One limitation of the new model is that it does not account for hydrostatic potential energy associated with the submergence of small bubbles, but this effect is expected to be small. It should also be noted that the kinetic energy of the gas jet is scaled for all working fluids at a constant time point of $t=0.4$ ms and not at a non-dimensional time formed using a capillary time $t_c = \sqrt{\frac{\rho_l R^3}{\sigma}}$ (Singh and Das 2021). This constant time point was chosen as it is the earliest time point at which the gas jet properties could be experimentally measured for all bubble sizes and working fluids. Further, using this early time point (i.e., before significant air entrainment or vortex ring formation) for all working fluids ensures that the gas jet morphology may be approximated by a simple cylinder and thus that the jet kinetic energy is captured in the

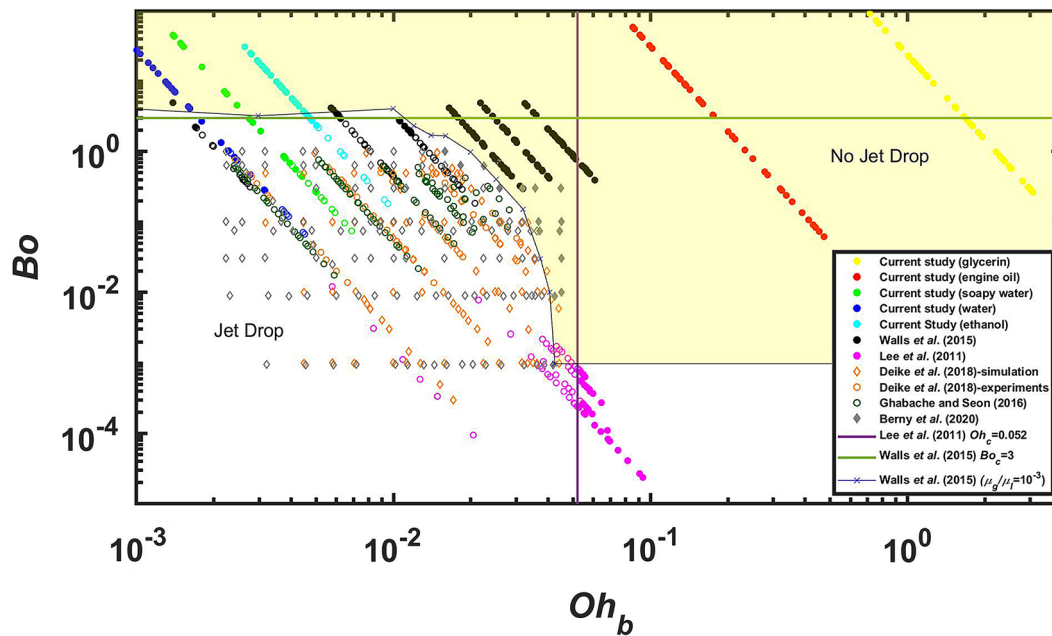


Fig. 9 Regime plot showing jet drop production as a function of bubble Ohnesorge number Oh_b and Bond number Bo for current and prior studies. Unfilled and filled symbols represent jet drop production and lack of jet drop production, respectively. Diamond and cir-

cle symbols indicate computational and experimental results, respectively. The yellow shaded area corresponds to the area with no jet drop production proposed by Walls et al. (2015)

scaling. In addition, the capillary time scale t_c may not be appropriate for the largest bubbles considered here, which are more than an order of magnitude larger than a .

While not the primary focus of this study, the data set collected here spans a wide range of bubble sizes and fluid properties and provides the opportunity to examine the scaling of jet drop formation. The soapy water data collected here also provide the opportunity to examine the possible effect of surfactants. Substantial prior research effort has gone into delineating the conditions under which a jet drop will be ejected from the Worthington jet, as well as the drop size, number, speed, and momentum (Duchemin et al. 2002; Ghabache et al. 2014; Walls et al. 2015; Ghabache and Séon 2016; Krishnan et al. 2017; Gañán-Calvo 2017, 2018; Deike et al. 2018; Lai et al. 2018; Brasz et al. 2018; Gordillo and Rodríguez-Rodríguez 2019; Blanco-Rodríguez 2020; Berny et al. 2020). In particular, Walls et al. (2015) investigated how both gravity and viscosity affect jet drop formation and demarcated jet drop production as a function of Bo and Oh_b . Other researchers have similarly demarcated jet drop production as a function of Bo and the Laplace number $La = \frac{\rho_l \sigma R}{\mu_l^2}$, where $La = Oh_b^{-2}$ (Deike et al. 2018; Brasz et al. 2018; Berny et al. 2020). Lee et al. (2011) experimentally found a critical bubble Ohnesorge number Oh_c of $Oh_c \approx 0.052 \pm 0.005$ above which no jet drop is expected to form at low Bo owing to viscous effects, and Walls et al. (2015) found $Oh_c \approx 0.04$,

both of which closely correspond to the critical Laplace number La_c of $La_c = 500$ (corresponding to $Oh_c = 0.044$) found by Deike et al. (2018). Further, Berny et al. (2018) experimentally found $La_c = 370$ and computationally found $La_c = 430$ (corresponding to $Oh_c = 0.052$ and $Oh_c = 0.048$, respectively). Similarly, a critical Bond number Bo_c of $Bo_c \approx 3$ has been proposed above which no jet drop forms at low Oh_b owing to the effect of gravity on bubble shape (Georgescu et al. 2002; Walls et al. 2015). In the intermediate region in which both gravity and viscosity are important, a boundary between regimes of $Bo \propto Oh_b^{-3}$ has been proposed (Walls et al. 2015).

Figure 9 shows the regime map of jet drop production as a function of Oh_b and Bo , including the data from the present study as well as prior experimental and computational findings from Lee et al. (2011), Walls et al. (2015), Ghabache and Séon (2016), Deike et al. (2018), and Berny et al. (2020). Data points are classified by whether or not a jet drop was produced and by whether the method was experimental or computational. The boundary between the shaded and unshaded areas corresponds to that found by Walls et al. (2015) for a gas-to-liquid viscosity ratio $\mu_g/\mu_l = 10^{-3}$. Vertical and horizontal lines corresponding to $Oh_c = 0.052$ and $Bo_c = 3$, respectively, also are plotted. The data collected in the present study match the previously established boundaries fairly well. The engine oil and glycerin experiments did not produce jet drops and largely fall at $Oh_b > 0.1$, where

no jet drop would be expected owing to viscous effects. In the region of high Bo and low Oh_b , gravity effects are most important in jet drop production and data are scarce. In this neighborhood (e.g., near Bo_c for $Oh_b < 10^{-2}$), a small discrepancy exists between the experimental results from the present study and prior computational results (Walls et al. 2015; Berny et al. 2020). Data for water, soapy water, and ethanol show a lack of jet drop production where prior simulations by Walls et al. (2015) suggest they should be produced, specifically at $Bo \approx 1$ for water and soapy water. This inconsistency suggests that the boundary may be found slightly lower than $Bo_c = 3$ or could be due to particular experiments failing to produce a jet drop because of bursting asymmetry or another cause. The effect of the surfactants in the soapy water bubbles also is not fully understood and may affect Bo_c (Néel and Deike 2021; Constante-Amores et al. 2021). For example, Constante-Amores et al. (2021) found that surfactants immobilized the air–water interface, resulting in shorter and slower Worthington jets that ejected fewer jet drops. This would tend to decrease the critical Bond and Ohnesorge numbers, and Oh_c for soapy water bubbles does seem lower than expected. A more detailed study of bubbles with and without surfactant near the Bo_c and Oh_c boundaries would be useful in this regard.

It is also interesting to compare the production and characteristics of the gas jet with those of the Worthington jet. The generation mechanisms of these two processes are naturally different. Gas jets are emitted because of the pressure difference between the interior and exterior of the bubble cap film and the rapid rupture of that film, whereas Worthington jets are generated by the collapse of the resulting sub-surface cavity which focuses capillary waves generated by the film rupture (Ghabache et al. 2014). Gas jet formation thus precedes Worthington jet formation in time. The speeds of gas jets and Worthington jets, however, may be of the same order of magnitude, though gas jet speeds are generally lower. Ghabache et al. (2014) found Worthington jet tip speeds decreased as a function of increasing bubble size and ranged from ~ 10 m/s for a $2R \approx 500$ μm bubble down to ~ 1 m/s for a $2R \approx 5$ mm bubble. Gas jet speeds across the same range increase from 0.28 m/s at $t = 1$ ms after bursting for a $2R = 440$ μm water bubble up to 2.9 m/s at $t = 0.4$ ms after bursting for a $2R = 5.2$ mm bubble (Dasouqi et al. 2020). Further, the gas jet and Worthington jets may interact with each other. Dasouqi et al. (2020) found that, for tiny bubbles bursting in water ($2R \approx 2$ mm), the upward impulse of the Worthington jet generated a secondary vortex ring at the base of the initial gas jet. Also, jet drops shed from the Worthington jet may travel through the mostly stationary jet and carry a trail of smoke in its wake, a phenomenon observed experimentally by Dasouqi et al. (2020) and in simulations (Singh and Das 2021).

One limitation of the current work is the difficulty of experimentally visualizing and measuring the gas expelled from tiny bursting bubbles. The smallest gas bubble examined here or in Dasouqi et al. (2020) was $2R = 440$ μm . At such small spatial and temporal scales, it is difficult to achieve sufficient smoke density within the bubble for a long enough period of time to visualize the resulting gas jet. Brasz et al. (2018) used microfluidics and Lee et al. (2011) used drop impact to observe jet drops generated by bubbles an order of magnitude smaller. It would be interesting to observe whether either the gas jet scaling $Re_{jet} = 126Bo^{0.5}$ found by Dasouqi et al. (2020) or the new one found here holds at these smaller scales. For example, a water bubble with $R = 20$ μm would be predicted to produce a gas jet with $Re_{jet} \approx 1$ by the original scaling law. Further, such a gas jet would be emitted through a miniscule hole owing to the small surface area of the highly submerged bubble's film cap. However, it is not clear whether the resulting gas jet could be visualized at this scale. Simulations accounting for both the liquid and gas components of bubble bursting would be useful in this regard, and progress has recently been made on this front (Deike et al. 2018; Singh and Das 2019, 2021).

4 Conclusions

In conclusion, we have visualized and quantified the release of gas jets from bursting bubbles comprised of water, soapy water, ethanol, engine oil, and glycerin bubbles across a wide range of bubble size (~ 0.5 – 44 mm) and four orders of magnitude of Bond number ($Bo = 0.06$ – 91). Gas jet speed and diameter increased with parent bubble size while film retraction speed decreased with parent bubble size. In general, low surface tension fluids (e.g., soapy water, ethanol) produced low-speed gas jets while high surface tension fluids (e.g., water) produced high-speed gas jets. Gas jet diameter was affected by both film retraction speed and bubble submergence in a complex way, with less submerged bubbles with quickly retracting films producing large jet diameters (e.g., ethanol), whereas more submerged bubbles with quickly retracting films producing much smaller diameter gas jets (e.g., water). A new scaling law was derived from the conservation of energy and compared to a prior scaling developed by Dasouqi et al. (2020). The new scaling reveals that bubble size and surface tension govern jet velocity and size, though bubble size is more important. Liquid density, which was varied only slightly in the current experiments, did not play a major role in determining jet behavior. Further, in contrast to other bubble bursting phenomena such as jet drop production, the initial gas jet behavior was not significantly affected by the liquid viscosity, which varied by almost a thousand-fold among tested fluids.

Acknowledgements The authors gratefully acknowledge Ali Alshamrani and Evan Williams for laboratory assistance and Ferhat Karakas for assistance with analysis.

Author Contributions A.D. and D. M. conceived and designed the experiment. A.D. and J. G. carried out experimental work and analyzed data. A.D. and D.M. wrote the manuscript. D.M. derived the scaling law. All authors approved the final manuscript.

Funding Funding was provided by a National Academies Gulf Research Program Early Career Research Fellowship to DWM.

Declarations

Conflict of interest The authors report no conflict of interest.

References

- Berny A, Deike L, Séon T, Popinet S (2020) Role of all jet drops in mass transfer from bursting bubbles. *Phys Rev Fluids*. 5(3):033605
- Blanchard DC (1963) The electrification of the atmosphere by particles from bubbles in the sea. *Prog Oceanogr* 1:73–202
- Blanco-Rodríguez FJ, Gordillo JM (2020) On the sea spray aerosol originated from bubble bursting jets. *J Fluid Mech*. <https://doi.org/10.1017/jfm.2019.1061>
- Brasz CF, Bartlett CT, Walls PL, Flynn EG, Yu YE, Bird JC (2018) Minimum size for the top jet drop from a bursting bubble. *Phys Rev Fluids* 3(7):074001
- Brenner MP, Gueyffier D (1999) On the bursting of viscous films. *Phys Fluids* 11:737–739
- Buchholz JHJ, Sigurdson LW (2000) The kinematics of the vortex ring structure generated by a bursting bubble. *Phys Fluids* 12:42–53. <https://doi.org/10.1063/1.870283>
- Buchholz JHJ, Sigurdson LW (2002) An apparatus to study the vortex ring structure generated by a bursting bubble. *Meas Sci Technol* 13:428–437. <https://doi.org/10.1088/0957-0233/13/4/302>
- Chojnicki KN, Clarke AB, Phillips JC, Adrian RJ (2015) Rise dynamics of unsteady laboratory jets with implications for volcanic plumes. *Earth Planet Sci Lett* 412:186–196. <https://doi.org/10.1016/j.epsl.2014.11.046>
- Constante-Amores CR, Kahouadji L, Batchvarov A, Shin S, Chergui J, Juric D, Matar OK (2021) Dynamics of a surfactant-laden bubble bursting through an interface. *J Fluid Mech*. <https://doi.org/10.1017/jfm.2020.1099>
- Culick FEC (1960) Comments on a ruptured soap film. *J Appl Phys* 31:1128
- Dasouqi AA, Murphy DW (2020) Gas escape behavior from bursting bubbles. *Phys Rev Fluids* 5:110502. <https://doi.org/10.1103/PhysRevFluids.5.110502>
- Dasouqi AA, Yeom GS, Murphy DW (2020) Bursting bubbles and the formation of gas jets and vortex rings. *Exp Fluids* 62:1–18. <https://doi.org/10.1007/s00348-020-03089-0>
- Day JA, Lease JC (1968) Cloud nuclei generated by bursting air bubbles at the air-sea interface. *Proc Int Conf Cloud Phys*. 49(5p2):593
- Debrégeas G, Martin P, Brochard-Wyart F (1995) Viscous bursting of suspended films. *Phys Rev Lett* 75(21):3886
- Deike L, Ghabache E, Liger-Belair G et al (2018) Dynamics of jets produced by bursting bubbles. *Phys Rev Fluids* 3:1–20. <https://doi.org/10.1103/PhysRevFluids.3.013603>
- Duchemin L, Popinet S, Josserand C, Zaleski S (2002) Jet formation in bubbles bursting at a free surface. *Phys Fluids* 14(9):3000–3008
- Gañán-Calvo AM (2017) Revision of bubble bursting: universal scaling laws of top jet drop size and speed. *Phys Rev Lett* 119(20):204502
- Gañán-Calvo AM (2018) Scaling laws of top jet drop size and speed from bubble bursting including gravity and inviscid limit. *Phys Rev Fluids* 3(9):091601
- Gekle S, Gordillo JM (2010) Generation and breakup of Worthington jets after cavity collapse. part 1. *Jet Formation J Fluid Mech* 663:293–330. <https://doi.org/10.1017/S0022112010003526>
- Georgescu SC, Achard JL, Canot E (2002) Jet drops ejection in bursting gas bubble processes. *European J Mech-B/Fluids* 21(2):265–280
- Ghabache E, Séon T (2016) Size of the top jet drop produced by bubble bursting. *Phys Rev Fluids* 1(5):051901
- Ghabache E, Antkowiak A, Josserand C, Séon T (2014) On the physics of fizziness: how bubble bursting controls droplets ejection. *Phys Fluids*. <https://doi.org/10.1063/1.4902820>
- Gordillo JM, Rodríguez-Rodríguez J (2019) Capillary waves control the ejection of bubble bursting jets. *J Fluid Mech* 867:556–571
- Iacono MJ, Blanchard DC (1987) An investigation of vortex rings from bursting bubbles. *Atmos Res* 21:139–149. [https://doi.org/10.1016/0169-8095\(87\)90004-4](https://doi.org/10.1016/0169-8095(87)90004-4)
- Jaw SY, Chen CJ, Hwang RR (2007) Flow visualization of bubble collapse flow. *J vis* 10:21–24. <https://doi.org/10.1007/BF03181797>
- Kientzler CF, Arons AB, Blanchard DC, Woodcock AH (1954) Photographic investigation of the projection of droplets by bubbles bursting at a water surface. *Tellus* 6:1–7
- Kim D, Yi SJ, Kim HD, Kim KC (2014) Visualization study on the transient liquid film behavior and inner gas flow after rupture of a soap bubble. *J vis* 17:337–344. <https://doi.org/10.1007/s12650-014-0217-2>
- Kobayashi T, Namiki A, Sumita I (2010) Excitation of airwaves caused by bubble bursting in a cylindrical conduit: experiments and a model. *J Geophys Res* 115:1–24. <https://doi.org/10.1029/2009J B006828>
- Krishnan S, Hopfinger EJ, Puthenveetil BA (2017) On the scaling of jetting from bubble collapse at a liquid surface. *J Fluid Mech* 822:791–812. <https://doi.org/10.1017/jfm.2017.214>
- Lai CY, Eggers J, Deike L (2018) Bubble bursting: Universal cavity and jet profiles. *Phys Rev Lett* 121(14):144501
- Lhuissier H, Villermaux E (2012) Bursting bubble aerosols. *J Fluid Mech* 696:5–44
- Liger-Belair G, Cilindre C, Gougeon RD et al (2009) Unraveling different chemical fingerprints between a champagne wine and its aerosols. *Proc Natl Acad Sci* 106:16545–16549. <https://doi.org/10.1073/pnas.0906483106>
- Mason BJ (1957) The oceans as source of cloud-forming nuclei. *Geophys Res* 62:148–155
- Murashita T, Ito A, Metoki T, Torikai H (2012) Flow visualization of extinguishing gas released from bursting soap bubbles. *Vis Mech Proc an Int Online J* 2:557–568
- Murphy DW, Li C, d’Albignac V et al (2015) Splash behaviour and oily marine aerosol production by raindrops impacting oil slicks. *J Fluid Mech* 780:536–577. <https://doi.org/10.1017/jfm.2015.431>
- Néel B, Deike L (2021) Collective bursting of free-surface bubbles, and the role of surface contamination. *J Fluid Mech*. <https://doi.org/10.1017/jfm.2021.272>
- Newitt DM (1954) Liquid entrainment 1. the mechanism of drop formation from gas or vapour bubbles. *Trans Inst Chem Eng* 32:244–261
- Pierson J-L, Magnaudet J, Soares EJ, Popinet S (2020) Revisiting the Taylor-Culick approximation: retraction of an axisymmetric filament. *Phys Rev Fluids*. <https://doi.org/10.1103/PhysRevFluids.5.073602>

- Poulain S, Villermaux E, Bourouiba L (2018) Ageing and burst of surface bubbles. *J Fluid Mech* 851:636–671. <https://doi.org/10.1017/jfm.2018.471>
- Prather KA, Bertram TH, Grassian VH, Deane GB, Stokes MD, DeMott PJ, Moffet RC (2013) Bringing the ocean into the laboratory to probe the chemical complexity of sea spray aerosol. *Proc Natl Acad Sci*. <https://doi.org/10.1073/pnas>
- Rogers WB (1858) On the formation of rotating rings by air and liquids under certain conditions of discharge. *Am J Sci Arts* 26:246–258
- San Lee J, Weon BM, Park SJ, Je JH, Fezzaa K, Lee WK (2011) Size limits the formation of liquid jets during bubble bursting. *Nat Commun* 2(1):1–7
- Savva N, Bush JWM (2009) Viscous sheet retraction. *J Fluid Mech* 626:211–240. <https://doi.org/10.1017/S0022112009005795>
- Singh D, Das AK (2019) Numerical investigation of the collapse of a static bubble at the free surface in the presence of neighbors. *Phy Rev Fluids* 4(2):023602
- Singh D, Das AK (2021) Dynamics of inner gas during the bursting of a bubble at the free surface. *Phys Fluids* 33(5):052105
- Song B, Springer J (1996) Determination of interfacial tension from the profile of a pendant drop using computer-aided image processing. *J Colloid Interface Sci* 184:77–91. <https://doi.org/10.1006/jcis.1996.0597>
- Stuhlman O (1932) The mechanics of effervescence. *J Appl Phys* 2:457–466. <https://doi.org/10.1063/1.1745071>
- Swinton AC, Beale E (1917) The bursting of bubbles. *Nature* 98:469. <https://doi.org/10.1038/099005b0>
- Taylor GI (1959) The dynamics of thin sheets of fluid III disintegration of fluid sheets. *Proc Royal Soc London Ser A Math Phys Sci*. 253(1274):313–321
- Teixeira MAC, Arscott S, Cox SJ, Teixeira PIC (2015) What is the shape of an air bubble on a liquid surface? *Langmuir* 31:13708–13717. <https://doi.org/10.1021/acs.langmuir.5b03970>
- Toba Y (1959) Drop production by bursting of air bubbles on the sea surface (II) theoretical study on the shape of floating bubbles. *J Oceanogr Soc Jpn* 15(3):121–130
- Torikai H, MurashitaItoTakumi TAM (2011) Extinguishment of a Laminar jet diffusion flame using a soap bubble filled with nitrogen gas. *Fire Saf Sci* 10:557–568. <https://doi.org/10.3801/IAF>
- Veron F (2015) Ocean Spray. *Annu Rev Fluid Mech* 47:507–538. <https://doi.org/10.1146/annurev-fluid-010814-014651>
- Walls PL, Henaux L, Bird JC (2015) Jet drops from bursting bubbles: How gravity and viscosity couple to inhibit droplet production. *Phys Rev E* 92(2):021002
- Zhang L, Lv X, Torgerson AT, Long M (2011) Removal of impurity elements from molten aluminum: a review. *Miner Process Extr Metall Rev* 32:150–228. <https://doi.org/10.1080/08827508.2010.483396>

Publisher's Note Springer Nature remains neutral with regard to jurisdictional claims in published maps and institutional affiliations.